

# ULTRASONIC ENERGY PROPAGATION IMAGING OF COMPOSITE STRUCTURES

Chen Ciang CHIA<sup>1</sup>, Jung-Ryul LEE<sup>\*1</sup>, Chan-Ik Park<sup>2</sup>, Jong Heon Kim<sup>2</sup>, Seung-Un Yang<sup>3</sup>  
<sup>1</sup>DEPT. OF AEROSPACE ENG., CHONBUK NATIONAL UNIV., Jeonju, Jeonbuk, Korea.  
<sup>2</sup>AERONAUTICAL TECHNOLOGY DIRECTORATE, AGENCY FOR DEFENSE  
DEVELOPMENT, Daejeon, Korea.  
<sup>3</sup>ENGINEERING RESEARCH CENTER, DACC CO. LTD., Wanju, Jeonbuk, Korea.  
\*Corresponding author: leejrr@jbnu.ac.kr

## Abstract

Laser ultrasonic wavefield and wave propagation imaging (UWPI) non-destructive evaluation (NDE) and structural health monitoring (SHM) methods deserve extra attention as they inherit many advantages from laser ultrasonic generation and they can reveal the location and severity of multiple damages. However, UWPIs lack frequency selectivity, hence we propose an ultrasonic energy propagation imaging (UEPI) method with frequency selectivity. It was built based on Q-switched laser, laser mirror scanner and wavelet transform technology. It generates Ultrasonic Energy Propagation Movie (UEPM) visible as ultrasonic energy field emerging from sensing location. Damages could be quantitatively evaluated from area with exclusive high ultrasonic energy concentration or abrupt energy field gradient change in UEPM. Frequency selectivity was demonstrated using an intact carbon fiber reinforced plastics plate. Result UEPMs of different frequencies showed propagation of either A0 mode alone or S0 and A0 modes together. NDE capability was demonstrated on an Al-alloy plate-foam core sandwich structure with debonding, and a quartz/epoxy plates-honeycomb core radome with impact damage. Results showed that location and size of defects could be easily evaluated by inspecting UEPMs. In conclusion, UEPI with frequency selectivity was developed as additional NDE method for UPI system. The ultrasonic frequency selection option was useful for ultrasonic modes isolation in generating UEPMs. Size and location of damages in scanned structure could be quantitatively evaluated using UEPM. The system is useful for NDE and SHM of engineering structures in the field.

Keywords: *Ultrasonic propagation imaging, laser ultrasonic, ultrasound mode selection, non-destructive evaluation of sandwich structure, radome impact damage.*

## 1. Introduction

Damage detection for aerospace, civil, and mechanical engineering infrastructure is of great importance because the integrity and functionality of these structures are essential for continuous development of the social economy. This is particularly true when these structures are getting larger to accommodate or support an increased number of users and becoming more complex as a result of integral production of advanced composite components for lower manufacturing and assembly cost [1]. Advanced non-destructive evaluation (NDE) and integrated structural health monitoring (SHM) systems ensure the safety of engineering structures, and at the same time facilitate condition-based maintenance, hence minimizing premature part change and maximizing the usage of structures according to their original designed purposes. Effective SHM or NDE methods must also have high throughput as well as the capability of generating intuitively understandable inspection results. High throughput is obviously necessary due to the increasing number and size of structures that require health monitoring or inspection. The ability to generate intuitively understandable inspection results is preferred to reduce the investment required to train highly skilled personnel and to avoid human error. SHM or NDE methods with imaging capability have great potential to fulfill these two requirements because an image could cover a large inspection area and reveal not only the existence of a single damage, but also the location and size of multiple damages. This information is crucial in deciding the most cost effective repair or replacement plan.

Many acousto-ultrasonic wave based SHM and NDE methods have imaging capability. Among them, laser-based ultrasonic wavefield and wave propagation imaging methods deserve extra attention because ultrasonic waves are sensitive to most material flaws, are not radiation hazardous, and provide many features for flaw characterization, while the laser offers non-contact remote characteristics for further exploitation. Full-field laser wavefield imaging, such as holography [2], generally requires highly diffusive target surfaces or laser illumination in dark environments and thus it has non-contact inspection capability but does not have remote automatic inspection capability. Further, it is very susceptible to parasite vibration. On the other hand, point-

wise laser imaging, such as scanning laser Doppler vibrometry [3], requires small laser incident angles and focusing for each sensing point. Typical  $\pm 20^\circ$  maximum incident angle greatly limits the ultrasonic measurement area in curved targets. Although auto-focusing is available, a 15 s focusing time is usually required at a sensing point with a different focal length. In addition, reflective film preparation on the target is needed for long-distance imaging. However, a robust ultrasonic wavefield imaging system can be realized when pulsed laser beams are used for ultrasonic generation. The pulsed laser beam offers many advantages, including: (i) fast non-contact ultrasonic generation at low pulse energy; (ii) remote sensing equipment for use in hostile environments, including the inspection of targets under elevated temperatures or containing hazardous materials; (iii) high spatial resolution; and (iv) the ability to inspect targets with complex surface geometries due to the allowable incidence angle of  $\pm 70^\circ$  [4]. To harness these advantages, an ultrasonic propagation imaging (UPI) technology was developed for the health monitoring scheme stimulating the integrated sensors in which a scanning pulsed laser and a fixed piezoelectric receiver were used [5]. The UPI technology consists of three parts; scanning ultrasonic generation, fixed ultrasonic reception, and damage evaluation algorithm. The scanning ultrasonic generation was improved by changes from a bulky and slow laser head scanner to a fast tilting mirror scanner [6], and then to high resolution galvanomotor type laser mirror scanner (LMS) [7]. The laser ultrasonic generator was improved from a Q-switched pulsed laser (QPL) [7], to a Q-switched continuous wave laser with a high signal repeatability and a high repetition rate in this work. Various ultrasonic reception techniques were also demonstrated, including direct PZT (lead zirconate titanate) sensor bonding and use of a fiber acoustic wave PZT sensor for inspection of target structures at elevated temperatures [7]. An electromagnetic interference-free optical UPI system combined with a fiber optic integrated SHM scheme was also realized using fiber acoustic wave grating sensors [8]. These UPI systems generate inspection results in the form of an ultrasonic wave propagation movie (UWPM), whose algorithm was previously described in detail [7]. UWPM is excellent for showing the presence and location of damage, but the appropriate selection of band-pass frequency gate is

very important because interaction of ultrasonic waves with structural damage or material property discontinuities may produce a scattering wavefield in which the frequency of the scattering wavefield could be significantly different than that of the incident wave. Scanning the target structure repeatedly using consecutive band-pass frequency gate may eventually reveal the existence of damage as well as the frequency of the scattering wavefield, but this should be the last option as the resources required would be enormous. Furthermore, ultrasonic waves are dispersive and a mixture of more than two modes is commonly seen in one wave. Each of these modes has different sensitivity for different structural attributes, therefore a frequency selection option would be advantageous.

In this work, aside of the improvement in UPI system hardware, we aimed to improve the damage evaluation algorithm part of UPI technology through introduction of a frequency-selectable Ultrasonic Energy Propagation Imaging (UEPI) method. This method enables ultrasonic mode selection through frequency selection, and can generate results in the form of Ultrasonic Energy Propagation Movie (UEPM) that can be seen as a simple ultrasonic energy field emerging from the sensor location. The UEPM is dramatically simpler than the UWPM, so it is much more intuitively understandable. Incorporating this function in the UPI system also means that multiple results corresponding to different frequencies can be generated using the data from one scanning, eliminating the need to scan the target structure repeatedly using different frequency band-pass settings.

## **2. UPI system and UEPI algorithm**

The UPI system is comprised of a QL, a galvanomotor-based LMS, an ultrasonic sensor, a programmable filter, a digitizer, and a computer for hardware control and image processing, as schematized in Figure 1. The QL has a wavelength of 1064 nm, a beam diameter of 0.7 mm at the laser head exit port, a divergence of 1.6 mrad and a pulse repetition rate up to 5 kHz. The LMS has two laser mirrors with working wavelengths of 1064 nm; each rotates by a galvanomotor about two

axes orthogonal to each other within an optical angle range of  $\pm 20^\circ$ . The QL fires optical pulses with durations of 30 ns at the LMS, and the mirrors of the LMS rotate to perform raster scans on the entire area of interest, i.e., to scan vertically downward, to step horizontally at the end of the downward movement, and then to scan upward for the next vertical scan. The speed of the mirror rotation is a function of LMS standoff distance, laser impinging interval  $\Delta$ , and the laser output repetition rate. For the case when standoff distance is 1 m,  $\Delta=2$  mm, and laser output repetition is 100 Hz, the mirror angular speed is 0.2 rad/s. The QL and LMS are synchronized for a constant laser impinging interval  $\Delta$  in both the vertical and horizontal axes.

When the laser beam impinges the surface of the target, an ultrasonic wave is created at the affected point. The wave propagates through the target and reaches a contact or non-contact ultrasonic sensor, which can be installed on the same or opposite side relative to scanning. Non-contact sensors such as air-coupled transducers and laser vibrometers can be used if the target surface does not allow any contact. Sensor establishment for the UPI system is greatly simplified even for a non-contact sensor that requires a fixed focal length, because one sensing point is sufficient for the UPI system. The signal from the sensor is amplified, filtered, and sampled for  $N$  number of data at a sampling time interval  $T$  using a digitizer. The function of the filter is to reduce random ambient noise.

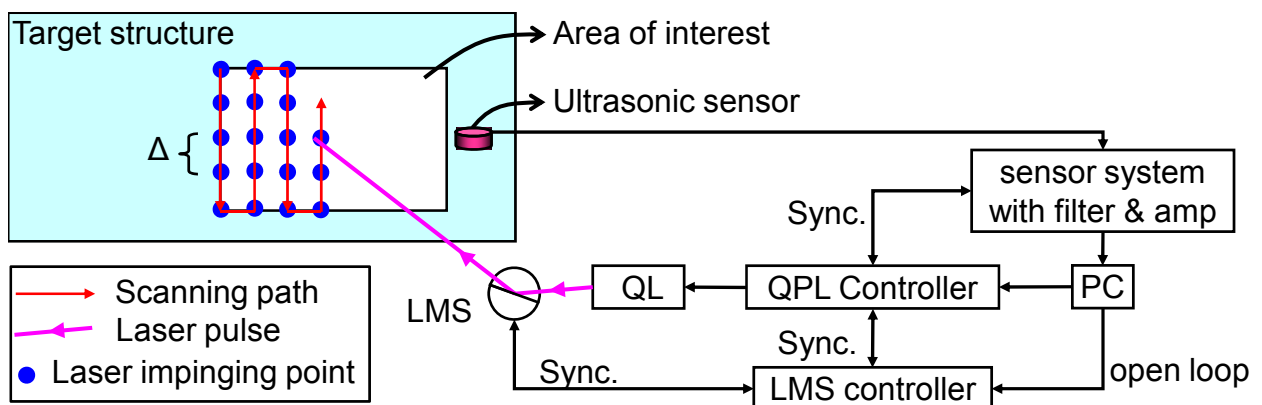


Figure 1. System schematic showing raster scan paths. LMS, laser mirror scanner; QL, Q-switched continuous wave laser; PC, computer.

Data processing for the UEPI method is carried out during the scanning. For every laser impinging point, one time domain ultrasonic signal will be acquired. The 1-D wave signals acquired already during the scanning are then converted into 2-D scalograms using wavelet transform (WT), as illustrated in Figure 2(a). This 2-D scalogram on the time versus frequency map contains the WT coefficient of all ultrasonic frequency components in the time domain. Extracting the WT coefficient at one particular frequency gives a 1-D energy signal (time versus WT coefficient). In Figure 2(a), one frequency selection line can be seen on the 2-D scalogram and the corresponding 1-D energy signal is given below the 2-D scalogram. The default frequency for 1-D energy signal extraction is the frequency that cuts through the peak of the wavelet coefficient in the 2-D scalogram for the signal of the first laser impinging point. The UEPM generated corresponds to this default frequency. If another frequency is specifically given, completing the rest of the data processing algorithm will generate a UEPM corresponding to the specified frequency. For cases of

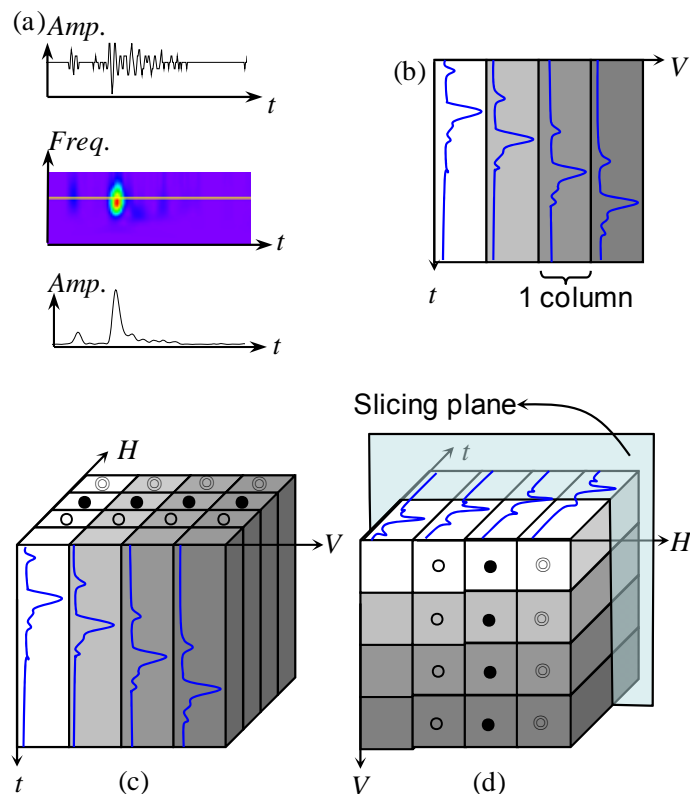


Figure 2. Algorithm for the generation of the UEPM at a specific frequency. (a) WT of an ultrasonic wave; (b) energy signals of one vertical scan path in one spreadsheet; (c) data for all scan paths; (d) slicing along the time axis of the 3-D data structure for UEPM snapshots.

both default frequency and specifically selected frequency, the frequency for 1-D energy signal extraction is constant throughout the scanning process. A self-normalized 1-D energy signal can be optionally used if time-of-flight (ToF) is the main concern for an inspection case.

As shown in Figure 2(b), the converted 1-D energy signal is stored as one column of data in a spreadsheet, and the other 1-D energy signals for all subsequent laser impinging points along the same vertical raster scan line are stored as new columns along the  $V$ -axis in the same spreadsheet. The 1-D energy signals for the subsequent vertical scan lines are saved along the  $H$ -axis in a new spreadsheet, creating the 3-D data structure shown in Figure 2(c). The  $n^{\text{th}}$  data of all of the signals is then mapped to the  $n^{\text{th}}$  spreadsheet with the same relative position on the spreadsheet as that of the laser impinging points on the scanned area. Graphically, the 3-D data in Figure 2(c) is rearranged to give the structure in Figure 2(d). It is then sliced along the time axis at each of the ultrasonic waveform sampling time intervals to yield  $N$  spreadsheets. Any of these spreadsheets plotted onto an intensity map with a suitable color scheme is seen as a static image of the ultrasonic energy propagating over the scanned area. The image generated from the  $n^{\text{th}}$  spreadsheet represents the snapshot at the  $nT$  instance of the ultrasonic energy propagation. Successively displaying the snapshots creates a UEPM visible as an ultrasonic energy field emerging from the sensor location.

With respect to post-image processing, the smoothness of a static image is increased using a noise reduction process called spatial averaging. This optional function is selected just before loading the spreadsheet data of the UEPM into the intensity map plot. A  $m \times m_k$  spatial averaging performs averaging on the data of  $m \times m$  adjacent points for  $k$  iterations. The parameter  $m$  is chosen for a small kernel, such as 3 or 5, while the number of iterations  $k$  is arbitrary. This iterative spatial averaging results in a Gaussian kernel instead of a box kernel in the case of the large kernel with one-time averaging [9]. We used  $3 \times 3_2$  spatial averaging for all experimental demonstrations in this paper.

### 3. Experimental demonstration

#### 3.1 Ultrasonic mode selection

To experimentally illustrate the concept of ultrasonic frequency selectivity and mode selectivity of the UEPM, we considered an intact 600 mm×600 mm×5 mm carbon fiber reinforced plastic (CFRP) plate with stacking sequence  $[45/90/-45/0_2/-45/0/90/0/45/0/45/90/-45]_s$ , as shown in Figure 3(a). The thickness of 5 mm corresponds to a thick skin part in general aircraft manufacturing. In other words, there were 12 plies of prepregs in the  $0^\circ$  orientation and six plies each of prepregs in the  $90^\circ$ ,  $45^\circ$  and  $-45^\circ$  orientations. The stacking sequence was controlled to have different elastic moduli in the  $x$  and  $y$ -axes ( $E_{xx} = 66.3$  GPa,  $E_{yy} = 43.1$  GPa) in the experiment shown in Figure 3(a). The LMS placed 2.2 m from the plate was used to reflect laser optical pulses with an energy of 1 mJ to scan an area  $400 \text{ mm} \times 400 \text{ mm}$  using  $\Delta = 2 \text{ mm}$  on the outer surface, also shown in Figure 3(a). It should be noted that the 1 mJ energy level is not in the plasma regime, which causes surface ablation [10], but is in the ultrasonic regime for the CFRP plate surface. Since the beam pulses were emitted with a repetition rate of 100 Hz and the number of scanned points was 40,401, the total scanning time was 404 s. An omni-directional, amplifier-integrated, and broadband piezoelectric transducer with a peak frequency of 300 kHz and a cut-off frequency of 2 MHz was bonded onto the center of the plate at the opposite side of the scanning. Signals were filtered using a band-pass filter from 100-250 kHz and were then sampled at 1.25 MS/s using  $N=255$ .

A 200 kHz UEPM was generated using default WT frequency setting. The sample scalogram in Figure 3(b) (acquired from the point marked with an asterisk in Figure 3(f)) shows that two distinct ultrasonic modes with different wavelength, i.e. the zeroth order plate-guided waves S0 mode and the A0 mode existed at this frequency. Snapshots of the UEPMs at 28  $\mu\text{s}$ , 40  $\mu\text{s}$ , 80  $\mu\text{s}$  and 128  $\mu\text{s}$  are given in Figures 3(c) to 3(f), respectively. The snapshots show both S0 mode and A0 mode. The S0 mode has higher group velocity than the A0 mode, hence the S0 mode could be seen far from the sensing location at early propagation time. The S0 mode is elliptical with the  $x$ -axis as its major axis because the ultrasonic arrival time in the  $x$  direction was less than that in the  $y$

direction due to the higher elastic modulus in the  $x$  direction controlled by the stacking sequence of the CFRP plate. The  $S_0$  mode velocity is proportional to the square root of the elastic modulus, whereas the  $A_0$  mode velocity is proportional to the fourth root of the elastic modulus [11]. This means that the effect of elastic modulus difference for the  $A_0$  mode velocity is much smaller than for the  $S_0$  mode, hence the near circular shape of the  $A_0$  mode is logical despite the difference of elastic modulus in the  $x$  direction and  $y$  directions.

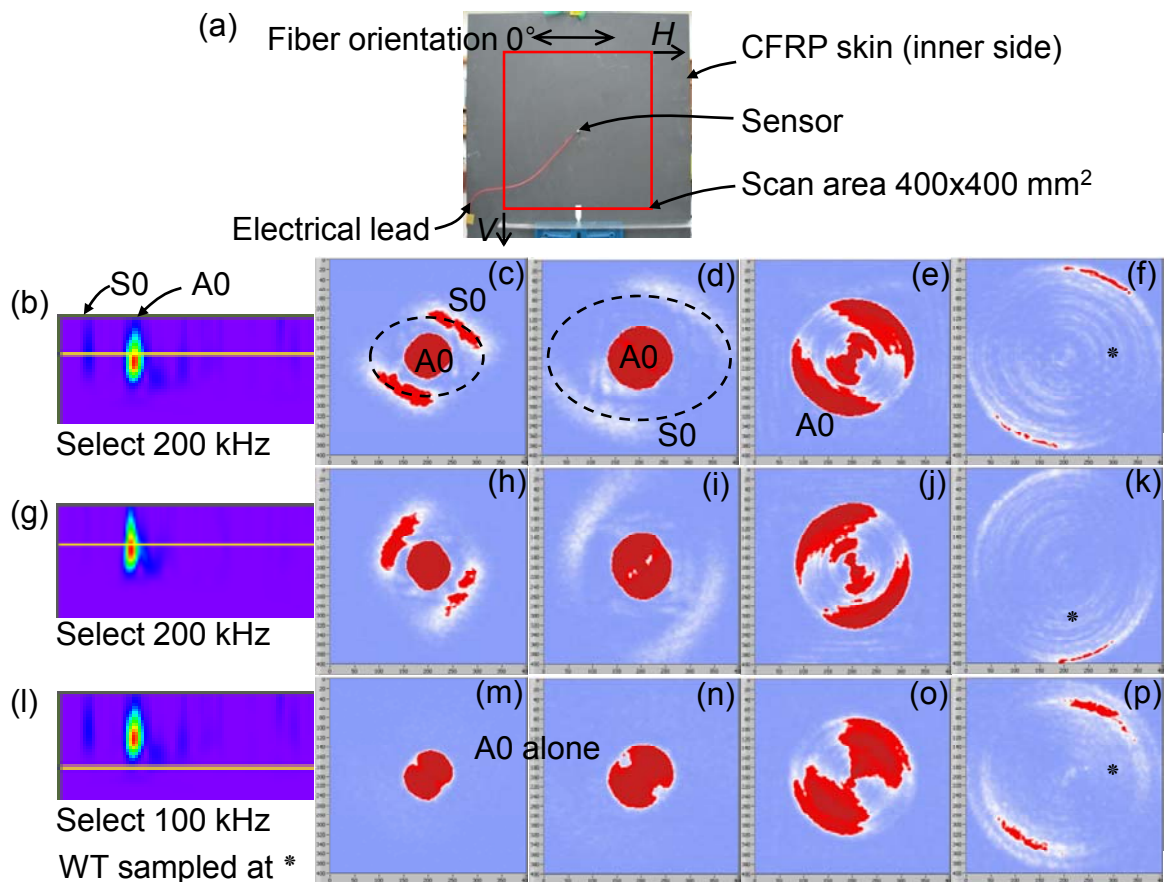


Figure 3. CFRP skin inspection result. (a) Experimental condition. (b) Sample scalogram with 200 kHz line and corresponding UEPM snapshots at (c) 28  $\mu$ s, (d) 40  $\mu$ s, (e) 80  $\mu$ s, and (f) 128  $\mu$ s. (g) Sample scalogram for rotated CFRP skin inspection with 200 kHz line and corresponding UEPM snapshots from (h) to (k). (l) Sample scalogram for 100 kHz case and corresponding UEPM snapshots from (m) to (p).

Higher energy could be observed in the upper right and lower left quadrants. In order to investigate the reason, scan was repeated with the specimen rotated 90° clockwise but with the sensor reinstalled for no rotation. In this case,  $E_{xx} = 43.1$  GPa and  $E_{yy} = 66.3$  GPa, resulted in an elliptical S0 mode with the y-axis as the major axis and higher energies in the upper left and lower right quadrants. The sample scalogram and UEPM snapshots at 28  $\mu$ s, 40  $\mu$ s, 80  $\mu$ s and 128  $\mu$ s are given in Figures 3(g) to 3(k), respectively. This verifies that the directivity was due to the first and last plies of prepregs in the 45° orientation, which in turn demonstrated that the UEPM can be useful for investigating material properties and microstructures. Using the data obtained for the case without specimen rotation, a UEPM was regenerated with 100 kHz WT for the isolation of A0 mode energy. The sample scalogram in Figure 3(l) shows the frequency selection line that was at the edge of the A0 mode. As shown in Figures 3(m) to 3(p), nearly circular energy propagation for only the A0 mode could be seen in the UEPM. The strong frequency selectivity of the UEPI is advantageous when ultrasonic mode selection and damage-related frequency isolation are required.

### *3.2 NDE of foam core sandwich structure using self-normalized UEPM*

To demonstrate the functionality of the UEPI method for defect evaluation, a sandwich structure comprised of a pair of 0.5 mm Al-alloy plates with thick foam core, and a 0.5 mm Al-alloy secondary protection plate epoxy-bonded to the first Al-alloy plate was inspected. At the center of the specimen, the first Al-alloy plate and the secondary protection plate were not bonded for a circular area with a diameter of 20 mm to simulate a frequent manufacturing defect, as schematized in Figure 4(a). The same piezoelectric transducer was bonded onto the scanning surface at the middle of the right edge of the scanned area. The LMS was used to scan an area 80 mm×80 mm on the specimen surface using  $\Delta=0.5$  mm. Signals were sampled at 12.5 MS/s using  $N=500$ . As shown in Figure 4(b), 600 kHz was selected for the UEPM generation so that the A0 mode was dominant in the result. The UEPM snapshots at 7.04  $\mu$ s, 12.80  $\mu$ s, and 18.72  $\mu$ s are shown in Figures 4(c) to 4(e), respectively. The self-normalization option for the 1-D energy signals was used

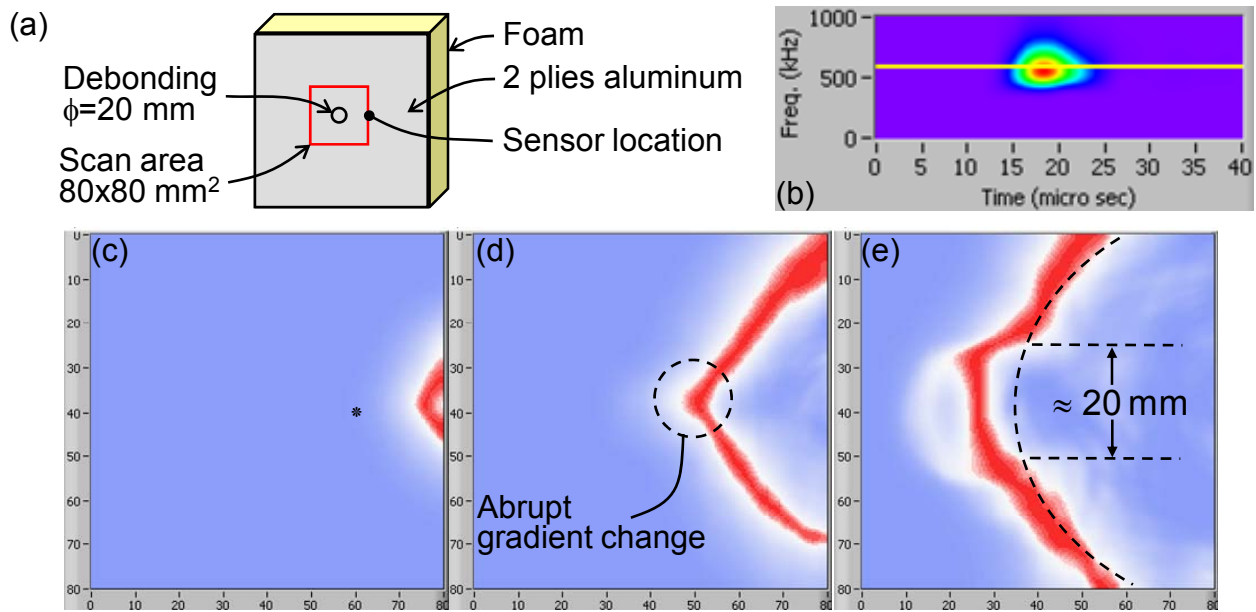


Figure 4. Bonding flaw inspection result. (a) Experimental conditions; (b) Scalogram showing 600 kHz as dominant frequency, taken from the point marked with asterisk in (c); Snapshots of normalized UEPM at (c) 7.04  $\mu$ s, (d) 12.80  $\mu$ s, and (e) 18.72  $\mu$ s.

in this demonstration because ToF information is important for debonding evaluation. A single arc-shaped ultrasonic energy field emerging from the sensor location is shown in Figure 4(c), but the gradient in the energy field changed abruptly in Figure 4(d). The length between the two points where the gradient changed abruptly suggests that the size of the defect was about 20 mm, as indicated in Figure 4(e). This demonstrated that both the size and the location of the defect could be evaluated using self-normalized UEPM.

### 3.3 NDE of honeycomb radome panel

A radome panel from a fighter jet pod made of quartz/epoxy plates and honeycomb core (Hexcel, cell size=9.5 mm) rectangular in shape (1445 mm $\times$ 245 mm $\times$ 9 mm) with all edges closed was inspected. LMS placed 1.5 m from the radome was used to reflect the laser optical pulses with approximately 10 mJ energy for scanning an area 100 mm $\times$ 100 mm on the outer skin using

scanning spatial interval 0.5 mm, as shown in Figure 5(a). Same PZT sensor was bonded on the inner skin at the bottom, also could be seen in Figure 5(a). A circular shape impact damage was made near the center of the radome using an energy of 5.42 J under the real installation condition of the boundary fastening, as illustrated in Figure 5(b). Ultrasonic A-scan showed that the damage has a diameter of 25 mm. Each ultrasonic signal was digitized using 500 points at sampling rate 1.25 MSa/s. UEPM was generated for 10 kHz and a sample scalogram was given in Figure 5(c). The UEPM generated could be seen as growth and shrink of area with exclusive energy concentration at the damage location. The snapshots at 180.0, 212.0, 264.0 and 398.4  $\mu\text{s}$  are given in Fig. 5(d) to (g) respectively. At 212.0  $\mu\text{s}$ , the energy concentrated area growth to the maximum size that could be enclosed by a circle of diameter  $\phi = 25$  mm, which is exactly the same size with the impact damage. This clearly demonstrates the effectiveness of location and size evaluation of an impact damage using UEPM.

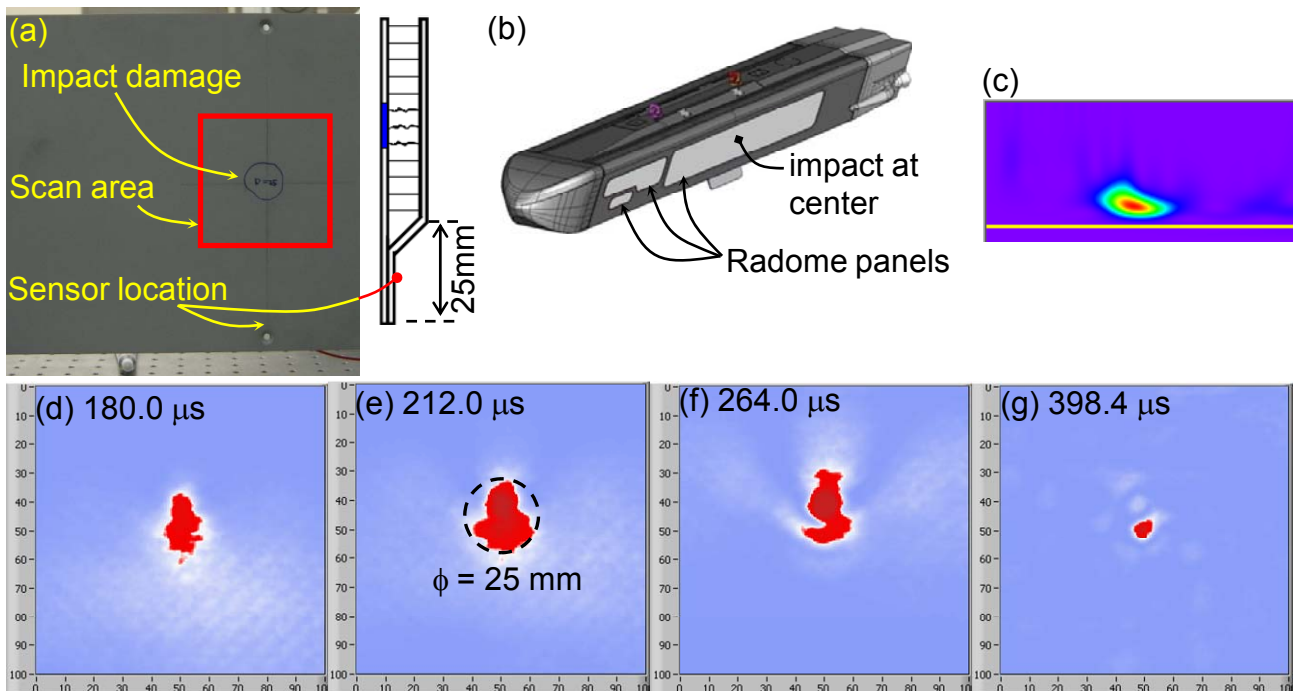


Figure 5. Radome inspection. (a) Experimental setup. (b) Illustration of jet fighter pod and the specimen radome panel. (c) Scalogram at center of scan area with 10 kHz frequency line. (d) to (g) UEPM snapshots. The area with exclusive energy concentration growth to maximum size of diameter  $\phi = 25$  mm at 212.0  $\mu\text{s}$ .

## 6. Conclusions

In conclusion, UEPI method with frequency selectivity was developed as additional damage evaluation method for UPI system. The ultrasonic frequency selection option was useful for the isolation of ultrasonic modes of interest in generating UEPMs. This was demonstrated on a CFRP plate by generating two UEPMs, one showing the energy propagation of only A0 mode, and another one showing the energy propagation of both S0 and A0 modes. Quantitative damage evaluation capability of the UEPI method was demonstrated using an Al-alloy plate-foam core sandwich structure with debonding defect, and a quartz/epoxy plates-honeycomb core jet fighter pod radome with impact damage. UEPM for each inspection case successfully revealed the location and size of damages with high accuracy. The UEPI method ameliorates the UPI system by giving it frequency selectivity option. Equipped with the conventional UWPI method and this newly developed UEPI, the UPI system becomes a robust NDE and SHM system useful for non-destructive quality evaluation and health monitoring of engineering structures in the field.

## Acknowledgement

We performed this study under the applied research project (UC080019JD) supported by the Agency for Defense Development in Korea. This paper was also supported by Korea Ministry of Land, Transport, and Maritime Affairs as the Haneul Project.

## References

- [1] Wilmes H, Kolesnikov B, Fink A and Kindervater C 2001 New design concepts for a CFRP fuselage *CFRP for future aircraft fuselage structures: Proc. DLR Institute of Structural Mechanics (Braunschweig, Germany, 24 October 2002)* (Published on CD-ROM, also available on the website of Institute of Structural Mechanics at [http://www.dlr.de/fa/Portaldata/17/Resources/dokumente/publikationen/2002/20\\_wilmes.pdf](http://www.dlr.de/fa/Portaldata/17/Resources/dokumente/publikationen/2002/20_wilmes.pdf))
- [2] Green R E, Jr. 2004 Non-contact ultrasonic techniques *Ultrasonics* **42** 9-16

- [3] Staszewski W J, Lee B C, Traynor R 2007 Fatigue crack detection in metallic structures with Lamb waves and 3D laser vibrometry *Meas. Sci. Technol.* **18** 727-39
- [4] Chia C C, Jang S-G, Lee J-R and Yoon D J 2009 Structural damage identification based on laser ultrasonic propagation imaging technology *Proc. Int. Conf. of SPIE Europe Optical Metrology-Optical Measurement Systems for Industrial Inspection VI (Munich, Germany, 17 June 2009)* Vol 7389
- [5] Lee J-R, Takatsubo J, Toyama N and Kang D-H 2007 Health monitoring of complex curved structures using an ultrasonic wavefield propagation imaging system *Meas. Sci. Technol.* **18** 3816-24
- [6] Chia C C, Lee J-R, Park J-S, Yun C-Y and Kim J H 2008 New design and algorithm for an ultrasonic propagation imaging system *Proc. Int. Conf. of DEFEKTOSKOPIE 2008 (Brno, Czech, 4-6 November 2008)* pp 63-70
- [7] Chia C C, Lee J-R and Shin H-J 2009 Hot target inspection using a welded fibre acoustic wave piezoelectric sensor and a laser-ultrasonic mirror scanner *Meas. Sci. Technol.* **20** 127003 (8pp)
- [8] Lee J-R and Yoon C-Y 2009 Development of an Optical System for Simultaneous Ultrasonic Wave Propagation Imaging at Multi-points *Experimental Mechanics* (Accepted: 7 September 2009, DOI 10.1007/s11340-009-9293-y)
- [9] Lee J-R 2005 Spatial resolution and resolution in phase-shifting laser interferometry *Meas. Sci. Technol.* **16** 2525-33
- [10] Davies S J, Edwards C, Taylor G S, Palmer S B 1993 Laser-generated ultrasound: its properties, mechanisms and multifarious applications *J. Phys. D:Appl. Phys.* **26** 329-48
- [11] Seale M D, Smith B T and Prosser W H 1998 Lamb wave assessment of fatigue and thermal damage in composites *J. Acoust. Soc. Am.* **103** 2416-24